Comparison of High-Side and Synchronous Trapezoidal Control Using XMC-Based Brushless DC Motor Controller for Pedelecs

Jomel Lorenzo, Jr.,* Jean Clifford Espiritu, Kristofferson Reyes, Isidro Marfori, and Noriel Mallari

Abstract — **This study aims to compare high-side and synchronous trapezoidal brushless DC (BLDC) control methods using an XMC-based motor controller for pedelecs. The electric bicycle implemented three different pedal-assist modes with varying human-to-motor power ratios and one throttle mode with the use of proportional-integral control. The study compares the efficiencies of two trapezoidal control methods through the throttle and pedal-assist mode. The data obtained shows that the high-side trapezoidal control is more efficient than the synchronous trapezoidal control in all modes implemented on the e-bike. This research opens possibilities to improve other BLDC control algorithms especially in terms of efficiency.**

Keywords: **Android, telemetry, PID, BLDC motor, trapezoidal motor control, Cortex-M0**

I. Introduction

Electric bicycles—or e-bikes—are lighter and smaller compared to motorcycles, yet they can give the comfort of riding one. To be able to get these benefits, a good motor controller for the electric bicycle is needed. Currently, e-bikes available in the market can assist riders when pedalling. Unfortunately, they do not have the capability to process complex data from the e-bike [1]. The study aims to improve the e-bike by focusing on the refinement of the motor controllers.

Electric bicycles would normally have a hub motor, which may be brushed or brushless [2]. In this study, the brushless DC (BLDC) motor is used. BLDC motors have favorable characteristics such as high efficiency, high speed ranges, and high torque-to-size ratios. However, they require complex control methods to commutate the motor as it requires six pulse width modulation (PWM) signals to operate. The BLDC motor would interface with a 32-bit microcontroller, which controls the MOSFETs (metal–oxide–semiconductor field-effect transistors) in order to adaptively drive the motor.

One similar study about pedelecs implemented smart features using an off-the-shelf motor controller from the market. However, the motor controller is treated as a black box, and the response of it is unpredictable [12]. This study designed the motor controller to control the motor's response effectively depending on the status of the e-bike.

From the previous study "Adaptive Speed and Power Control for a Pedelec Using an ARM Cortex-M0 Microcontroller," the motor controller already implemented three modes of pedal assist (executive, mid, and sport) that control the target power depending on human input and throttle mode, which control the target speed of the user [6]. This study implemented two trapezoidal BLDC control signals to the motor controller and compared the difference of the two control methods in terms of efficiency of different modes discussed from the previous study.

II. Design Consideration and Methodology

A. Infineon XMC 32-Bit ARM Microcontroller

The researchers used Infineon's XMC1302 with a 32-bit ARM Cortex-M0 microprocessor inside (Fig. 1). This microcontroller is used specifically for motor control by having the hardware capable of giving PWM signals of over 20kHz [8].

Jomel Lorenzo, Jr.,* Jean Clifford Espiritu, Kristofferson Reyes, Isidro Marfori, and Noriel Mallari, De La Salle University-Laguna

*(e-mail: jomel_lorenzo@dlsu.edu.ph)

Fig.1. XMC1302 boot kit microcontroller.

B. BLDC Motor Control Using MOSFETs

The commutation of the BLDC motor functions appropriately by applying the concept of an inverter. Basically, an inverter is a switching control that converts direct current to alternating current or vice versa [3]. There are several types of inverters; however, one of the types of inverters used to drive a BLDC motor is the full-wave three-phase inverter. The inverter consists of six switching devices similar to the diagram shown below (Fig. 2) [5]. These MOSFETs are controlled with a pulse controller, which generates switching pulse signals. The signals generated consist of varying PWM, which controls the switching MOSFETs.

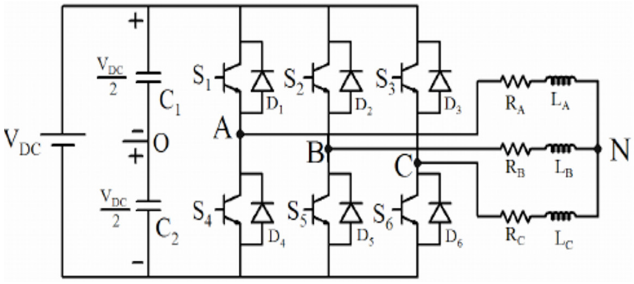

Fig. 2. Three-phase inverter.

C. High-Side and Synchronous Trapezoidal BLDC Control Methods

The BLDC motor has its advantages; however, it requires complex algorithms to operate [3]. Using a three-phase inverter made of MOSFETs, the operation of the BLDC motor can be controlled using PWM signals to move the motor to its desired position. Hall sensors would determine the current position of the motor [15]. Table I and Figure 3 show the high-side trapezoidal control signals applied in the inverter for proper commutation of the BLDC motor while Table II and Figure 4 show the synchronous trapezoidal control signals that have the same function of high-side with an additional inverted PWM in the low-side MOSFETs [10][11].

TABLE I
HIGH-SIDE COMMUTATION PATTERN WITH HALL SENSOS

No.	Hall Sensor			Input MOSFET Gate Signals					
	U	V	W	UH	UL	VH	VL	WH	WL
1	L	L	H	L	L	PWM	L	L	H
2	L	H	H	PWM	L	L	L	L	H
3	L	H	L	PWM	L	L	H	L	L
4	H	H	L	L	L	L	H	PWM	L
5	H	L	L	L	H	L	L	PWM	L
6	H	L	H	L	H	PWM	L	L	L

TABLE II
SYNCHRONOUS COMMUTATION WITH HALL SENSORS

No.	Hall Sensor			Input MOSFET Gate Signals					
	U	V	W	UH	UL	VH	VL	WH	WL
1	L	L	H	L	L	PWM	iPWM	L	H
2	L	H	H	Pwm	iPWM	L	L	L	H
3	L	H	L	PWM	iPWM	L	H	L	L
4	H	H	L	L	L	L	H	PWM	iPWM
5	H	L	L	L	H	L	L	PWM	iPWM
6	H	L	H	L	H	PWM	iPWM	L	L

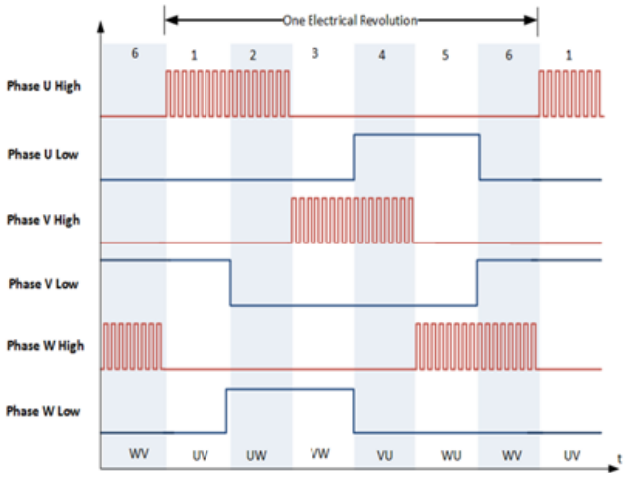

Fig. 3. High-side trapezoidal control signals.

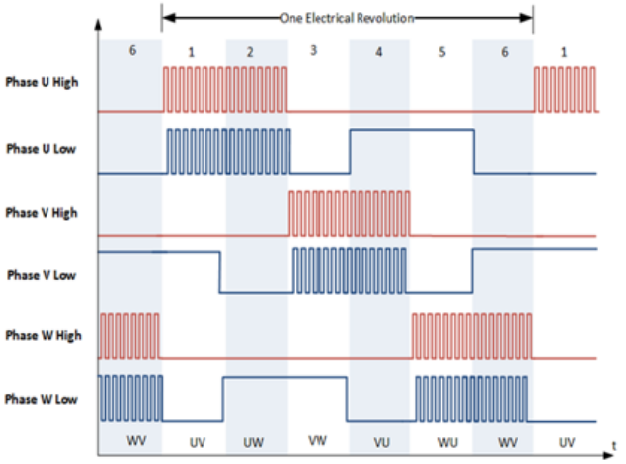

Fig. 4. Synchronous trapezoidal control signals.

D. Dead Time

Dead time is necessary in implementing the synchronous control because two PWMs are used in the same phase in the inverter [9]. Without the dead time, the high-side and low-side MOSFETs will be shorted; thus, a high current will flow, which in turn will destroy the MOSFETs. The researchers implemented a 150-ns dead time in the signals to prevent the short circuit from happening. Figures 5 and 6 show implemented dead time in the signals, and they also show that the point of intersection of the two signals will not trigger the MOSFET to be switched on. Therefore, the MOSFETs in the inverter will not generate a short circuit during operation.

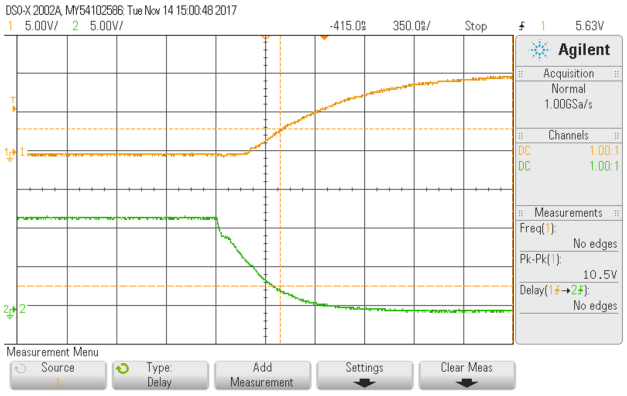

Fig. 5. Dead time in rising edge of the signal for high-side MOSFET and falling edge of the signal for low-side MOSFET.

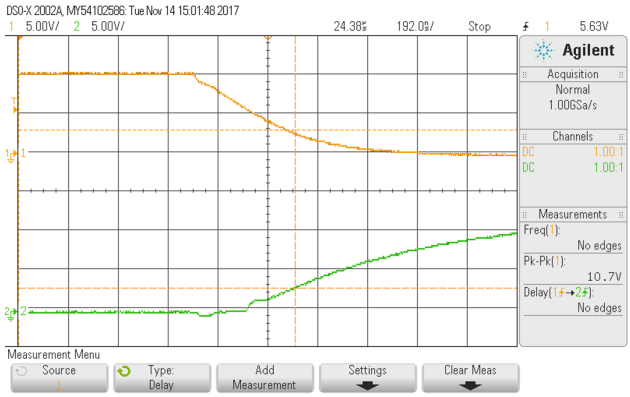

Fig. 6. Dead time in falling edge of the signal for high-side MOSFET and rising edge of the signal for low-side MOSFET.

E. Vehicle Kinematic Formula and Theoretical Power Computation

Power is needed to move the electric bicycle at any given speed. Equation 1 shows the factors that affect the required power to move the electric bicycle [4]. The human or the motor must exert more power when riding uphill, over rough roads, and in windy places.

$$P_{theo} = \frac{P_{drag} + P_{fric} + P_{hill}}{Eff} \quad (1)$$

Equation 1 can be expanded to consider the characteristics of the e-bike and the rider resulting to Equation 2. The efficiency can be computed when P_{theo} is equated to input power (P_{in}), which is equal to the product of battery current and voltage.

$$P_{theo} = \frac{0.5\left(pAV^2C_D\right)V + \left(\left(m_B + m_R\right)gC_R\right)V + \left(m_B + m_R\right)g\left(V\sin\theta\right)}{eff} \quad (2)$$

where

V = *velocity (m/s)*
m_V = *weight of the bicycle (kg)*
m_D = *weight of the rider (kg)*
g = *acceleration due to gravity (9.8 m/s²)*
C_{RR} = *coefficient of rolling resistance (unitless)*
p = *air density (1.2 kg/m³)*
A = *bicycle and rider frontal area (m²)*
C_D = *coefficient of drag*
θ = *inclination angle in degrees from horizontal plane*
Eff = *e-bike efficiency ($0 < Eff \leq 1$)*

F. Pedal-Assist and Combining Human Power and Motor Power

Pedal-assist is a concept that is achieved only when the motor is stimulated when the user is pedaling the electric bicycle. In order to detect if the user is pedaling the electric bicycle, a cadence sensor using hall magnets is utilized. To improve the response further, a torque sensor is used to determine the input human power into the system. Since the human power is identified, it is now possible to implement more advanced control algorithms that target a specific ratio between the human power and the motor power. The three ratios used for this study are the executive, mid, and sports modes. Executive mode makes the motor do 70% of the power output while the human is only 30% of the power output. Mid mode ensures that both the motor and the human equally contribute to the total power of the system. Sports mode makes the human do 70% of the power output while the motor only does 30% of the power output.

$$P_h = \tau * (2\pi * \omega)(3) \quad (3)$$

where

P_h = human power (W)
τ = torque (Nm)
ω = cadence (rps)

$$\tau = F * \frac{r}{\pi} \int_{-\frac{\pi}{2}}^{\frac{\pi}{2}} \cos(x)\, dx \quad (4)$$

where

τ = torque (Nm)
F = human force (N)
r = crank radius (m)

G. Speed Control

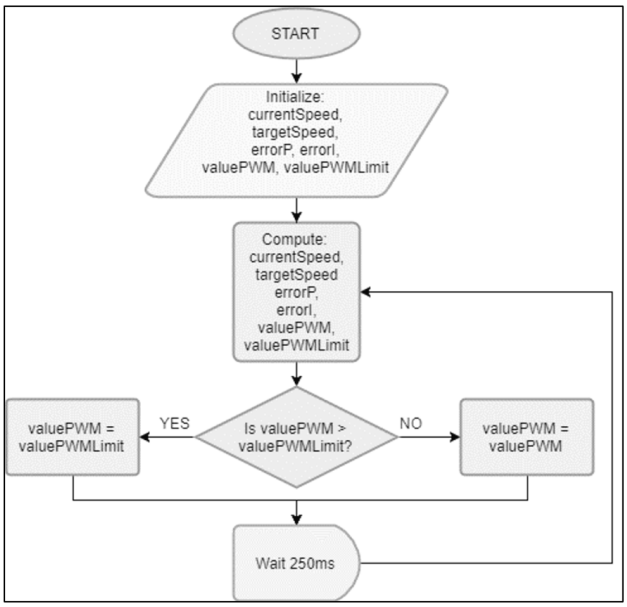

Fig. 7. Flowchart for speed control.

In this section, the researchers implemented a proportional-integral speed control algorithm for throttle mode that will target the desired speed of the user and maintain its current speed when the target speed is reached. See flowchart used in targeting speed for throttle mode (Fig. 7) [6].

A. Power Control

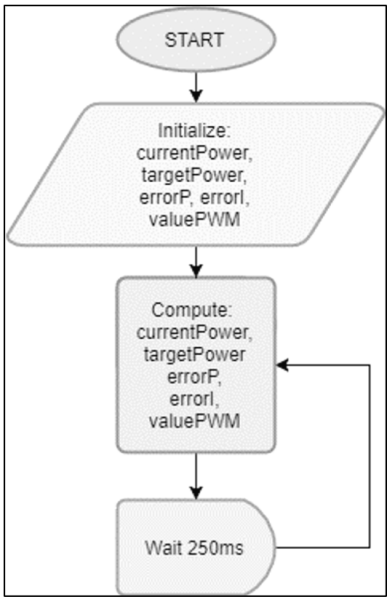

Fig. 8. Flowchart for power control.

In this section, the researchers implemented proportional-integral power control algorithm for pedal-assist mode. The target power will be adjusted depending on the mode used by the user and its peddling behavior. See flowchart used in controlling the motor power for pedal-assist mode (Fig. 8) [6].

I. MOSFET Characteristics

The researchers used IPP04N12N13G, a MOSFET that is capable of blocking 120 V during off condition and can let 120 A pass during on condition [13]. The battery voltage used in the study is 36 V, and choosing a breakdown voltage for a MOSFET must be twice of its input as a rule of thumb. This MOSFET can also be applied to 48-V battery systems.

J. Gate Driver Response Time and Determination of Switching Frequency

In this study, an Infineon MOSFET gate driver (MGD), 2EDL05N06PF, is used for translating the switching signals from the microcontroller to a higher voltage to fully drive the MOSFET [14]. MGDs are important in the circuit as they provide isolation to the high-power side and the low-power side of the circuit. In addition to that, they can support 20-kHz PWM frequency as an input by adjusting the value of the bootstrap capacitor to 1 uF. Figure 9 shows the circuit configuration of a MGD in one phase.

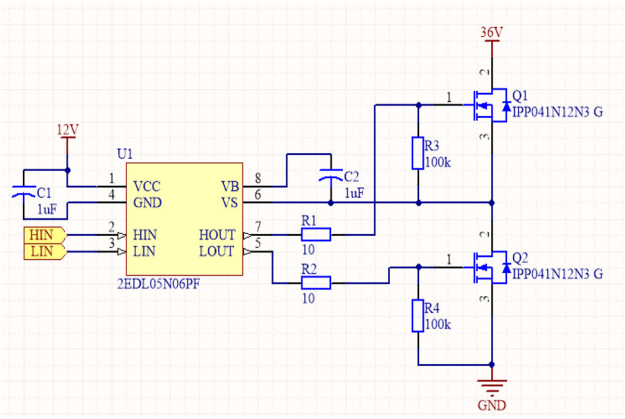

Fig. 9. MOSFET gate driver configuration.

III. RESULTS AND DISCUSSION

This section contains the efficiency testing of the two trapezoidal BLDC control methods. The testing setup was done on a flat road to eliminate the power needed to overcome slopes.

A. High-Side Trapezoidal

Figures 10, 11, and 12 show the efficiency of the e-bike operating in three pedal-assist modes using high-side trapezoidal control. The calculated average efficiency is 78.01%, which indicates efficient motor control of the system.

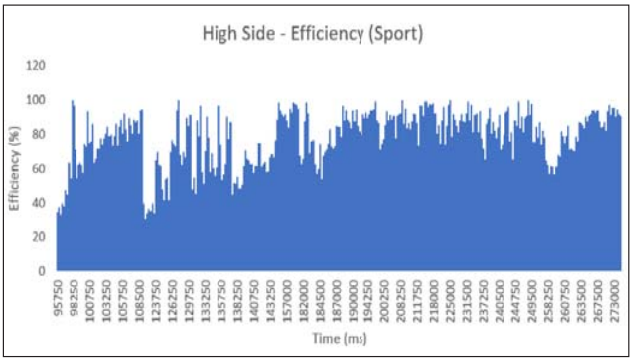

Fig. 10. Efficiency versus time (sports mode, high-side).

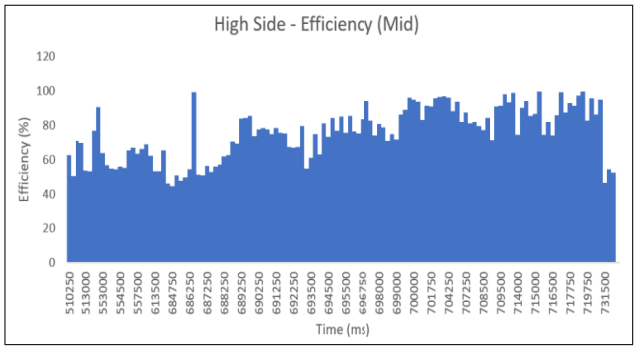

Fig. 11. Efficiency versus time (mid node, high-side).

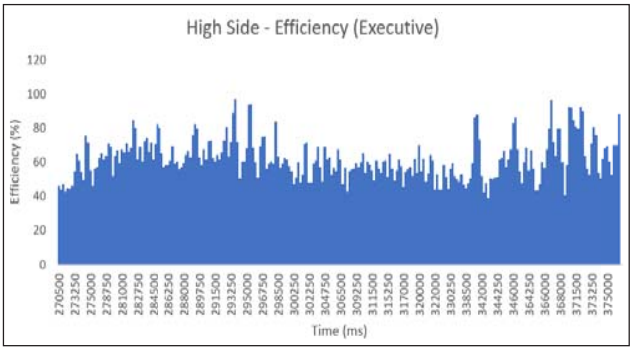

Fig. 12. Efficiency versus time (executive mode, high-side).

Likewise, Figure 13 shows the efficiency of the e-bike when operating in smart throttle. The calculated average efficiency in this case is 70.11%. This was attained through the use of an advanced state machine algorithm.

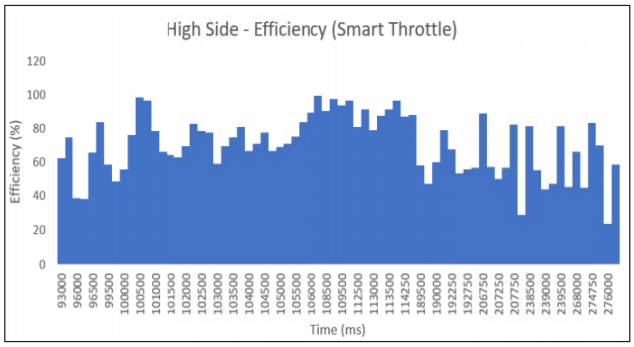

Fig. 13. Efficiency versus time (smart throttle, high-side).

B. *Synchronous Trapezoidal Control*

In the synchronous trapezoidal control method, Figures 14, 15, and 16 show the efficiency of the e-bike using the same testing setup in the high-side, and it is operated also in three pedal-assist modes, while Figure 17 shows the efficiency in the throttle mode that also used the same algorithm in the high-side.

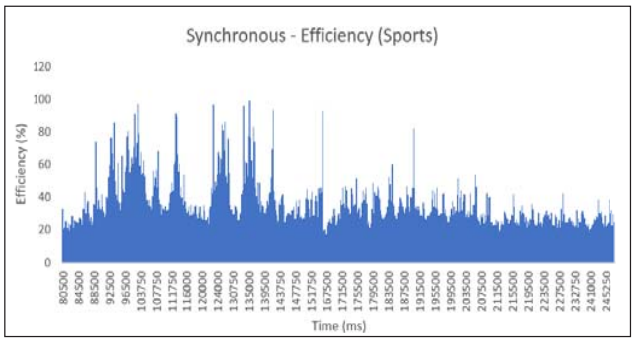

Fig. 14. Efficiency versus time (sports mode, synchronous).

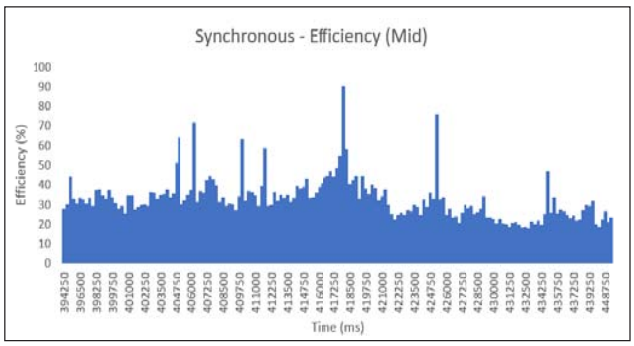

Fig. 15. Efficiency versus time (sports mode, synchronous).

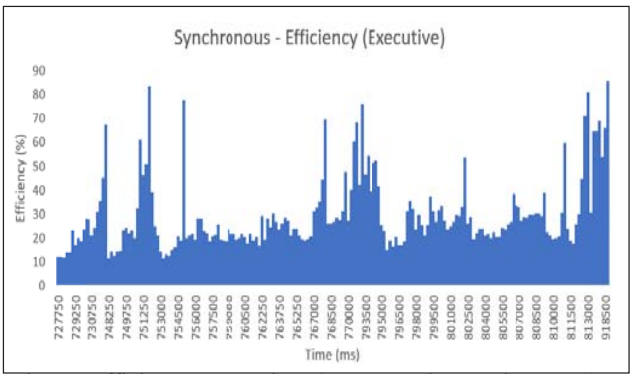

Fig. 16. Efficiency versus time (sports mode, synchronous).

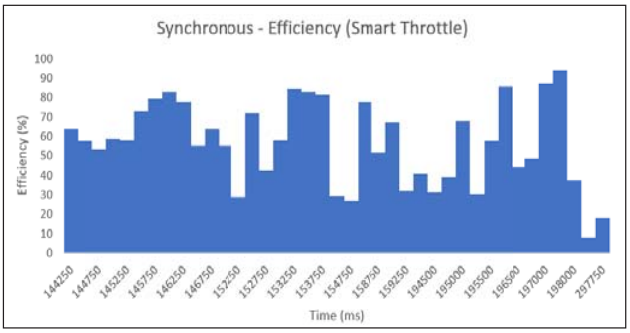

Fig. 17. Efficiency versus time (sports mode, synchronous).

C. *Comparison of the Two Control Methods*

Each graph in the data obtained from two trapezoidal control methods was used to get the average of the values in order to compute for efficiency of the system in each mode. Table II shows the summary of the efficiencies from two trapezoidal control methods.

TABLE III
SUMMARY OF DATA FOR THE EFFICIENCY OF BOTH CONTROL METHODS

Mode	Synchronous	High-Side
Sports	36.5%	78.01%
Mid	32.7%	75.41%
Executive	29.27%	61.97%
Throttle	56.25%	70.11%
Average	**38.68%**	**71.375%**

CONCLUSIONS

In summary, the study was able to compare two trapezoidal control methods in terms of efficiency. It was found that high-side trapezoidal control is more efficient than the synchronous trapezoidal control by a factor of 2,

whereas the average of efficiency across all modes of high-side control method is 71.38% while the average efficiency of synchronous control method is 38.68% across all modes. This result shows that if the e-bike is used in synchronous control and it only traverses 10 km in one full charge of the battery, then operating it using the high-side control method could travel 20 km in one full charge of the battery because of its efficiency. When driving the motor, the synchronous control method produces louder acoustic noise compared to the high-side trapezoidal control. This was caused by high torque ripple present in synchronous control, which is inefficient in flat roads [7].

At the end of the study, the researchers were successful in implementing two BLDC control methods and comparing their difference in terms of efficiency to determine the best control method to be used for the e-bike.

V. Recommendation

The researchers recommend adjusting the dead time, which can change the response of the synchronous trapezoidal control. Also, adding smart features such as Bluetooth connectivity to the smartphone and battery prediction will improve the overall response of the e-bike.

Acknowledgment

The researchers would like to thank Mr. Antonio and Infineon for giving us support through the power MOSFETs and the XMC1300 Boot Kit. We would also like to thank Engr. Noriel Mallari for assisting us with the leap from Arduino to an industry-grade microcontroller. Finally, we would like to thank Nyfti Inc. for providing the bicycle chassis used for the study.

References

[1] "About Us | Faraday Electric Bikes," *Faraday Bikes*, 2017. [Online]. Available: https://www.faradaybikes.com/about/. [Accessed: Oct. 6, 2017].

[2] "Sine-wave controllers, making hub-motors super quiet," *ElectricBike.com*, 2017. [Online]. Available: https://www.electricbike.com/sine-wave/. [Accessed: Oct. 7, 2017].

[3] T. Rahman, S. Motakabber, and M. Ibrahimy, "Design of a switching mode three phase inverter," *2016 IEEE International Conference on Computer and Communication Engineering (ICCCE)*, pp. 155–160, 2016.

[4] A. Gross, C. Kyle, and D. Malewicki, "The aerodynamics of human-powered land vehicles," *Scientific American*, vol. 249, no. 6, pp. 142–152, 1983.

[5] T. Erfidan, S. Urgun, and B. Hekimoglu, "Low cost microcontroller based implementation of modulation techniques for three-phase inverter applications," *MELECON 2008—The 14th IEEE Mediterranean Electrotechnical Conference*, pp. 541–546, 2008.

[6] K. Reyes, J. Lorenzo, J. Espiritu, P. Sacdalan, N. Mallari, and I. Marfori, "Adaptive speed and power control for a pedelecusing an ARM Cortex-M0 Microcontroller," 2017.

[7] L. Jianjun, X.Yongxiang, and J.Zou, "A study on the reduction of vibration and acoustic noise for brushless DC motor,"*in 2008 International Conference on Electrical Machines and Systems,* pp. 561–563*,* 2008.

[8] Infineon, "XMC1300 Microcontroller Series for Industrial Applications ARM Cortex-M0 32-bit processor core," XMC1302 Datasheet, May 2014.

[9] K. Denny, "PWM control and dead time insertion," *Hackaday.io*, 2018. [Online]. Available: https://hackaday.io/project/3176-gator-quad/log/11741-pwm-control-and-dead-time-insertion. [Accessed: Jan. 1, 2018].

[10] Texas Instruments, "DRV8308 Brushless DC Motor Controller," Texas Instruments Incorporated, Feb. 2014. [Revised: Nov. 2017].

[11] Renesas. "BLDC motor control algorithms," *Renesas Electronics Singapore*, 2018. [Online]. Available: https://www.renesas.com/en-sg/solutions/key-technology/motor-control/motor-algorithms/bldc.html. [Accessed: Jan. 1, 2018].

[12] N. Mallari, J. Macaraig, D. Navarrete, and I. Marfori, "Smart motor controller using model-based algorithm for control of pedal-assisted electric bicycle," 2016.

[13] Infineon, "2EDL05N06PF EiceDRIVER™ Compact High voltage gate driver IC," Infineon Technologies, Jan. 2016.

[14] Infineon, "IPP041N12N3 G OptiMOS Power-Transistor," Infineon Technologies, April 2014.

[15] J. Zhao and Y. Yu, "Brushless DC motor fundamentals application note,"*Monolithic Power Systems, Inc.* , 2011.